P6.9

NEW QUANTIFICATION OF HODOGRAPH SHAPE IN NOCTURNAL TORNADO ENVIRONMENTS AND ITS APPLICATION TO FORECASTING: OBSERVATIONS

AMANDA K. KIS[1]

School of Meteorology, University of Oklahoma, Norman, OK

JERRY M. STRAKA

School of Meteorology, University of Oklahoma, Norman, OK

Submitted to Weather and Forecasting

[1] Corresponding author address: Amanda K. Kis, University of Oklahoma, School of Meteorology Suite 5900, 120 David L. Boren Blvd., Norman, Oklahoma 73072, <Email: akkis@ou.edu>

ABSTRACT

Hodographs associated with supercells are typically described as straight or curved. The climatologically observed hodograph with tornado outbreaks is a hybrid of these two extremes, with a curved shape in the lowest 1–3 km AGL that denotes veering of the environmental wind with height, and a straight shape above that indicates a unidirectional environmental wind with height. In contrast to this mean hodograph, a bent low-level hodograph shape is found in proximity of nearly 75% of nocturnal tornadoes while less than 25% of nocturnal tornadoes have archetypal curved or straight low-level hodographs. The bent low-level hodograph is similar to the “sickle” and “kinked” that have been noted with destructive tornadoes and indicates strong speed shear and very little veering of the environmental wind with height in roughly the lowest kilometer above the surface.

Bent and straight low-level hodographs in proximity of nocturnal tornadoes are associated with exceptionally large 0–1 km AGL storm relative environmental helicity (SREH). In order to examine the effects of hodograph shape on in SREH in the lowest kilometer, 5-m AGL storm-relative inflow, 0–1 km AGL bulk vertical wind shear, and critical angles are computed for each hodograph in the sample. While straight hodograph feature the strongest 5-m AGL storm-relative inflow and largest 0–1 km AGL vertical wind shear, bent low-level hodographs occur in environments with much larger components of horizontal streamwise vorticity.

The layers of strong speed shear adjacent to the surface that are indicated by bent low-level hodographs are apparently caused in part by overhead low-level jets (LLJ). The speeds of jet maxima correlate very well with measures of low-level bulk vertical wind shear in proximity

of nocturnal tornadoes with bent low-level hodographs. However, the heights of jet maxima correlate poorly with the heights of hodograph bends.

1. Introduction

Unlike daytime tornadoes, nocturnal tornado environments are characterized by marginal instability (Kis and Straka 2010; hereafter KS10). The lack of lift by instability is countered by strong vertical pressure gradient accelerations associated with exceptionally strong low-level vertical shear of the horizontal wind. Such strong low-level vertical wind shear is likely consequent of overhead low-level jets (LLJ; Stull 1988), which may be driven by the inertial oscillation, synoptically embedded, or a combination of both.

The low-instability/high shear environments in which nocturnal tornadoes generally form has been widely omitted from tornado studies, possibly because they do not nearly match the instability-rich environments that have been observed with many destructive tornadoes and successfully employed in numerical simulation tornado studies (e.g. Wicker and Wilhelmson 1993, 1995; Grasso and Cotton 1995). The accumulated omissions of nocturnal tornado environments have led to a daytime-tornado bias in the literature. This bias is especially dangerous when one considers that nocturnal tornadoes represent only 25.8% of U.S. tornadoes yet are linked to 42.5% of tornado-related fatalities (Ashley et al. 2008). Improved operational nocturnal tornado forecasting could elevate public awareness of nocturnal tornadoes by permitting increased coverage in advance of overnight severe weather. However, the misplaced application of observations from daytime-tornado studies to potentially tornadic nighttime severe weather might increase the risk of missed events. In addition, the use of forecast tools derived from daytime-tornado climatologies to nocturnal tornado forecasting may misguide forecasters and diminish the accuracy of long-term nocturnal tornado forecasts.

To evaluate the tornado potential of severe weather environments, forecasters turn in part to the shapes of hodographs. Hodograph shapes vary with the nature of the vertical shear of the horizontal wind. Since vertical wind shear is typically much larger in nocturnal tornado environments than in the environments of late afternoon and early evening tornadoes, it seems likely that average hodograph shape would also differ between these regimes. In section 2 of this paper, low-level hodograph shape is rigorously defined with the use of quantified speed and directional shear. In an attempt to understand the influence of different vertical wind shear regimes on tornadic environments, components of the storm relative environmental helicity (SREH; Davies-Jones et al. 1990) equation are analyzed and presented in section 3 and signals are identified. The results are discussed in section 4, and recommendations to forecasters are made in section 5.

2. Methodology & dataset

1) SAMPLE SELECTION AND CRITERIA

KS10 sampled 241 nocturnal tornadoes that occurred between 1 January 2004 and 31 December 2006. They defined nocturnal tornadoes as those occurring between 0900 p.m. and 0700 a.m. Local Solar Time. Eighty-four nocturnal tornadoes in KS10's sample had proximity 20-km Rapid Update Cycle Version 2 (RUC-2; Benjamin et al. 1998) 0-h analysis gridpoint soundings from at least one site, and are used herein to construct a sample suitable for examining proximity hodographs. Of these 84 tornadoes with proximity soundings, 56 were weak (F0–F1) (Table 1) and 28 were significant (F2–F5) (Table 2). See KS10 for comments on the use of RUC-2 gridpoint soundings and the criteria for proximity. For these tornadoes, surface-based (SB-), mixed layer (ML-), and effective parcel (EFF-; Thompson et al. 2007) convective available potential energy (CAPE), convective inhibition (CIN), and lifting condensation level (LCL) were calculated as indicators of instability. Velocity difference, which is referred to herein as bulk shear, and SREH in the 0–1, 0–3, 0–6, and 0–8 km AGL and effective inflow layers were calculated as indicators of vertical wind shear.

RUC-2 gridpoint soundings are well suited for analysis of low-level hodograph shape. Small vertical spacing near the surface, with 2-, 5-, 8-, and 10-hPa spacing in the first four layers and an explicit model calculation level at 5-m AGL (Benjamin et al. 2001), allows the 20-km RUC-2 to resolve fine scale vertical boundary layer features. In addition, RUC-2 gridpoint soundings are available at a much larger spatial and temporal density than are observed soundings.

Hodographs for each proximity sounding were plotted with the Skew-T Hodograph Analysis and Research Program software (NSHARP; Hart and Korotky 1991). The hodograph shape criteria are described in the following sub-sections.

2) HODOGRAPH BACKGROUND

Supercell storm motion is determined partly by advection by the mean wind in the cloud-bearing layer and partly by the interaction of the convective updraft and the vertically sheared environment (Bunkers et al. 2000). The latter interaction causes supercell motion to deviate from the mean wind and move across the environmental vertical wind shear (Rotunno and Klemp 1982, 1985; Weisman and Klemp 1982, 1984, 1986; Klemp 1987). Deviant motion varies from supercell to supercell in consequence of the differing environmental vertical wind shears that they encounter, and the differing proportions of directional and speed shears in turn determine the environmental hodograph shapes. In supercell environments hodograph shapes are traditionally categorized within a spectrum that extends from straight to curved (Weisman and Klemp 1982, 1984). Perfectly straight hodographs indicate pure speed shear (Markowski and Richardson 2006). With straight hodographs, split pairs of supercells form and storm motion is off of the hodograph, with the supercell on the right (left) side of the hodograph moving to the right (left). Perfectly curved curved hodographs indicate pure directional shear (Markowski and Richardson 2006). With curved hodographs, storm motion is towards the concave side of the hodograph. A clockwise-turning environmental wind with height favors right-moving supercells and a counter-clockwise-turning environmental wind with height favors left-moving supercells (e.g. Weisman and Klemp 1984). The effects on supercells of a turning environmental wind with height are most influential for low-level curvature (Klemp and Wilhelmson 1978, Rotunno and Klemp 1982), and the correlation between the updraft and vertical vorticity increases as low-level curvature increases (Weisman and Rotunno 2000). While bulk wind shear measurements for use by forecasters is typically calculated over depths ranging from 1–8 kilometers above the surface, it is the shear over the lowest 1–3 km AGL that is most important for creating horizontal vorticity that can be tilted vertically by storms and used in mesocyclogenesis and possible tornadogenesis (Davies and Johns 1993, Johns et al. 1993). This is reflected in the fact that vertical wind shear parameters measured in the lowest 1–3 km AGL are much better discriminators of tornadic environments than are vertical wind shear parameters measured over greater depths (e.g. Rasmussen and Blanchard 1998, Rasmussen 2003, Thompson et al. 2003).

The climatologically observed hodograph with tornado outbreaks, based on 1200 and 0000 UTC soundings, reflects veering of the wind in the inflow layer and unidirectional shear above in the free atmosphere, and thus is curved in a clockwise manner in a layer adjacent to the surface and predominantly straight above about 700 hPa (Maddox 1976; Fig. 1). However, preliminary review by the authors of hodograph in proximity of nocturnal tornadoes identified only a few cases that resembled the climatological tornadic hodograph. Instead, in most cases a "bent" shape was identified in the lowest kilometer. Though this shape has been noted with several destructive tornadoes (Thompson and Edwards 2000, hereafter TE00; Miller 2006, hereafter M06; Esterheld and Guiliano 2008, hereafter EG08), it has not been investigated nearly as thoroughly as have the curved and straight hodographs typically found with supercells and tornadoes.

While hodographs can appear bent for various vertical wind profiles, a review of the relevant literature reveals that the bent hodograph shape typically indicates a layer of strong speed shear adjacent to the surface that is topped by a layer that is dominated by directional shear (TE00, M06, EG08). In some cases, the layer of strong speed shear is very shallow, with bulk vertical wind shear greater than 10 m s^{-1} in the lowest 250–400 m AGL (e.g. M06, EG08). Above these layers to a height of 1-km AGL, winds veer between 30–40 degrees. However, very little additional data is presented in these studies as to the amount of speed and directional shear below and above hodograph bends, respectively, and what is given is mainly presented as anecdotal evidence.

This regime of shallow strong speed shear topped by strong directional shear will be rigorously examined in the following sections of this paper, and quantifications of the amount of speed and directional shears will be presented. The next sub-section details definitions of hodograph shape that will best detect this particular regime. Investigation of this seemingly common hodograph shape in nocturnal tornado environments may shed light on the type of strong low-level vertical wind shear in which nocturnal tornadoes tend to occur.

3) A RIGOROUS HODOGRAPH SHAPE DEFINITION

Straight hodographs occur in environments of pure speed shear, and curved hodographs occur in environments of pure directional shear. Many bent hodographs are hybrids of the archetypal straight and curved hodograph regimes, and separate a shallow layer adjacent to the surface where speed shear is dominant and a layer above where directional shear is dominant (TE00, M06, EG08). Though bent hodographs may occur in other shear regimes (see Fig. 5 of M06), the regime of shallow speed shear topped by directional shear seems most common and will thus define the bent low-level hodographs examined herein.

Hodograph shape in the lowest 1.5-km AGL is rigorously defined in an effort to understand the effects of vertical wind shear on hodograph shape and streamwise vorticity (Davies-Jones 1984). The 1.5-km AGL layer is chosen in part because hodograph bends are generally found below 1.5-km AGL (e.g. M06, EG08) and in part to prevent contamination of inflow layer wind profiles with features in the free atmosphere.

Hodograph shape in the lowest 1.5-km AGL is defined with use of speed and directional shears (see Appendix A for detailed shear calculations). Straight low-level hodographs (SH) were defined as those hodographs with speed shear on average at least an order of magnitude greater than directional shear continuously throughout the lowest 1.5-km AGL. Curved low-level hodographs (CH) were defined as those with speed shear on average at least an order of magnitude smaller than directional shear continuously throughout the lowest 1.5-km AGL. Bent low-level hodographs (BH) hodographs were defined as those with a layer adjacent to the surface of speed shear on average and continuously at least an order of magnitude greater than directional shear that was located directly beneath a layer of directional shear at least an order of magnitude greater than speed shear. For the straight portion of bent hodographs, measurements of speed sheer at least an order of magnitude larger than directional shear were required over a minimum of three data points that started from the explicitly calculated 5-m AGL level to define hodograph shape. Post-analysis, it was revealed that all of the straight portions of bent low-level hodographs were defined using at least 4 data points, and over 75% were defined using at least 6 data points.

KS10 noted that nocturnal tornadoes were often coincident with overhead LLJs. LLJ speed at 850 hPa correlated well with 0–1 km AGL bulk vertical wind shear, and in consequence KS10 suggested that strong bulk vertical wind shear measurements typically found in the low-levels of nocturnal tornado proximity environments could be resultant of overhead LLJs. KS10 used RUC-2 0-h analysis data to estimate the speeds of overhead LLJs at 850 hPa. These estimates can be made more exact for the entire sample herein with the RUC-2 proximity soundings. For each proximity sounding, jet maxima speeds and heights above the surface were identified in a manner similar to Whiteman et al. (1997). However, Whiteman et al. (1997) required a minimum drop-off of 5 m s^{-1} from the jet maximum to the next minimum. While this criterion was feasible for their study that specifically investigated the intertially driven nocturnal LLJ, it is not applicable to the LLJs herein that appear to be synoptically embedded. Instead, no minimum drop-off is required, and the speed maximum closest to the surface is used as the LLJ maximum. These criteria identified an overhead LLJ with each nocturnal tornado.

3. Results

The hodograph shape criteria detailed above identified 62 (43 weak, 19 significant) nocturnal tornadoes with BH, three nocturnal tornadoes with CH (2 weak, 1 significant), and five nocturnal tornadoes with SH (0 weak, 5 significant) (Tables 1 and 2). The shape criteria for bent low-level hodographs detected many very straight speed shear layers below hodograph bends (Fig. 2a) similar to those shown in TE00, M06, and EG08. The criteria also detected slightly curved speed shear layers below hodograph bends (Fig. 2b), and bends that were more gradually kinked than the sharp bends shown in M06 and EG08. Curved and straight low-level hodographs were similar to their archetypes (Fig. 2c, d). Two nocturnal tornadoes with hodograph shapes in the lowest 1.5-km AGL that did not fit any of these three shape categories were labeled as “unidentifiable” and were not included in subsequent calculations.

Nine weak and 3 significant nocturnal tornadoes were associated with multiple hodographs that had different archetypal shapes in the lowest 1.5-km AGL. In these cases, the tornadoes were not categorized into specific shape categories, but their hodographs were separately grouped into their respective shape categories for further calculations. When taken collectively, the 82 nocturnal tornadoes with identifiable hodograph shapes were associated with 145 proximity soundings. These soundings corresponded to 114 BH, 15 CH, and 16 SH. The 114 soundings with BH were associated with 81 weak nocturnal tornadoes and 33 significant nocturnal tornadoes; the 15 soundings with CH were associated with 14 weak nocturnal tornadoes and 1 significant nocturnal tornado; and the 16 soundings with SH were associated with 3 weak nocturnal tornadoes and 13 significant nocturnal tornadoes.

The disparity in sample sizes among soundings with BH, CH, and SH should be kept in mind in the following discussions about SREH.

a. Hodograph bend statistics

Eighty seven-percent of the hodograph bends occurred below 1-km AGL (Fig. 3). The height of hodograph bends above the surface provided some discrimination between weak and significant nocturnal tornadoes, as evidenced by the slight offset in boxes in Fig. 3. Two-tailed p values were on the order of 8×10^{-5}, which indicates that the results are highly statistically significant. (A p value assumes that the null hypothesis is true and is the probability of obtaining a result at least as extreme as the one that was actually observed.) More than three-quarters of hodograph bends with weak nocturnal tornadoes were located below 800 m AGL, whereas about half of hodograph bends with significant nocturnal tornadoes were located above 800 m AGL. When shallow stable boundary layers were present, bends were generally located several hundred meters above the stable layer inversions. Nearly 70% of BH had an average wind direction below bend height of south-southeasterly, southerly, or south-southwesterly. As will be discussed in the next sub-section, average wind directions were likely due to the presence of south or southwesterly intertially driven or synoptically embedded LLJs.

b. Storm relative environmental helicity

Environmental horizontal vorticity can be partitioned into streamwise and crosswise components, where streamwise (crosswise) vorticity is parallel (perpendicular) to the storm-relative inflow vector (Davies-Jones 1984). The streamwise component is incorporated into storm updrafts to produce supercells. In an environment of given horizontal environment vorticity, the maximum amount of streamwise environmental horizontal vorticity is tilted vertically by and incorporated into storm updrafts when storm motion is parallel to and oriented oppositely of the horizontal environmental vorticity vector. These motions can be evaluated through calculation of SREH. Storm relative environmental helicity is a measure of the amount of streamwise vorticity in the inflow layer that can be incorporated into a storm updraft and is calculated as:

$$SREH = -\int_0^h k \cdot (\mathrm{v} - \mathrm{c}) \times \frac{\partial v}{\partial z} \partial z ,$$

where h is the chosen height above the surface of the inflow layer, **v** is an environmental wind vector, and **c** is the storm motion vector (Davies-Jones et al. 1990).

Storm relative environmental helicity in the layer adjacent to the surface is directly proportional to the area swept out between the surface and a height on a hodograph (see Fig. 1), and is thus directly dependent on low-level hodograph shape. Curved hodographs are typically associated with the largest amount of SREH. However, for the sample herein, bent and straight low-level hodographs were on average associated with much larger SREH in the lowest kilometer above the surface (hereafter $SREH_{0\text{-}1}$) than were curved low-level hodographs. Three-quarters of nocturnal tornadoes with BH and about 80% of nocturnal tornadoes with SH had $SREH_{0\text{-}1}$ greater than 200 $m^2\ s^{-2}$ (Fig. 4). The majority of CH had $SREH_{0\text{-}1}$ less than 200 $m^2\ s^{-2}$ (Fig. 4). Differences among hodograph shapes were not as apparent for SREH integrated over larger depths or over the effective inflow layer.

In the following sub-sections, several terms in the SREH integrand are examined to investigate the influence of the different shear regimes that are represented by different low-level hodograph shapes on streamwise vorticity in a tornadic storm's proximity environment. The height, h, over which SREH is calculated is set to 1-km AGL. Storm motion, $\mathbf{c}$, is calculated with the Internal Dynamics Technique (Bunkers et al. 2000) for right-moving supercells. The lowest wind measurement in RUC-2 gridpoint soundings is explicitly calculated at 5-m AGL (Benjamin et al. 2001) and is chosen as the 5-m AGL environmental inflow vector, $\mathbf{v}$.

1) COMMENT ON STORM MOTION CALCULATIONS

The use of the Internal Dynamics Technique to calculate storm motion rather than using observed storm motion likely contributes to errors in SREH calculations, in particular from calculations of the storm-relative inflow vector and the critical angle. Calculation of storm motion with the Internal Dynamics Technique results in a mean vector error magnitude (MVE) between 4.1 m s^{-1} (Bunkers et al. 2000) and 4.3 m s^{-1} (Ramsay and Doswell 2008). The authors could not find any statistics available on the average direction error.

2) 0–1 KM AGL BULK SHEAR AND SFC–BEND BULK SHEAR

Tornado climatologies with late afternoon/early evening biases have found that most tornadoes occur in environments of moderate low-level shear, with 0–1 km AGL bulk shear less than 13 m s^{-1} (e.g. Thompson et al. 2003, Craven and Brooks 2004). However, 75% of weak nocturnal tornadoes and nearly 90% of significant nocturnal tornadoes in KS10's sample and the subset examined herein had 0–1 km AGL bulk shear greater than 13 m s^{-1}. Evidently, nocturnal tornadoes tend to occur in environments of exceptionally strong low-level shear.

Bulk 0–1 km AGL vertical wind shear was greater than 20 m s^{-1} for about 75% of nocturnal tornadoes with SH and between 13–20 m s^{-1} for more than 75% of nocturnal tornadoes with BH and SH (Fig. 5). A large portion of the bulk 0–1 km AGL shear with BH was found beneath the hodograph bends (hereafter SFC–bend bulk vertical wind shear). This is evidenced by the substantial overlap in interquartile ranges between 0–1 km AGL and SFC–bend bulk shear in both weak and significant nocturnal tornadoes with BH in Fig. 6. Both bulk 0–1 km AGL and SFC–bend vertical wind shear discriminated well between weak and significant nocturnal tornadoes. Two-tailed p values were on the order of 10^{-5}, which indicates that the results are highly statistically significant. As in KS10, bulk shear thresholds in this study are estimated for the samples of weak and significant nocturnal tornadoes, and are chosen so that at least 75% of the significant nocturnal tornadoes occurred with values of the parameter greater than the threshold. KS10 found that 18 m s^{-1} of 0–1 km AGL bulk vertical wind shear discriminates well between weak and significant nocturnal tornadoes. Estimates from Fig. 6 suggest that 19 m s^{-1} of SFC–bend bulk shear discriminates well between sampled weak and significant nocturnal tornadoes with bent hodographs, and values higher than this threshold indicate an increasing possibility of significant nocturnal tornadoes. This discriminator can be combined with those found by KS10 to further aid in nocturnal tornado forecasting.

Low-level jets may strengthen vertical wind shear below the height of their jet maxima (e.g. Maddox 1993, French and Parker 2010). It seems likely that the large 0–1 km AGL and SFC–bend bulk shears found with all of these cases was influenced by overhead LLJs. Bulk 0–1 km AGL shear exhibited high correlation with jet maxima speeds for nocturnal tornadoes with BH (.77), CH (.78), and SH (.95). Speeds of LLJ maxima were on average substantially higher for SH (29 m s^{-1}) than for BH (21 m s^{-1}) and CH (15 m s^{-1}). Thus, it seems likely that 0–1 km AGL bulk shear was greater for the majority of nocturnal SH than for the majority of BH and CH (Fig. 5) due at least in part to the higher LLJ speed maxima with SH than with BH and CH. Speeds of LLJ maxima also exhibited high correlation with SFC–bend bulk shear (.82), and thus it seems likely that overhead LLJs in large part responsible for the large speed shear found below hodograph bends.

3) 5-M AGL STORM RELATIVE INFLOW

Storm-relative inflow, v – c, at 5-m AGL was substantially higher for nocturnal tornadoes with SH than with BH and CH (Fig. 7). About three-quarters of nocturnal tornadoes with SH occurred with 5-m AGL storm-relative inflow greater than 17 m s^{-1} while about three-quarters of nocturnal tornadoes with BH and CH occurred with 5-m AGL storm-relative inflow less than 17 m s^{-1}.

Additionally, storm-relative 5-m AGL storm-relative inflow discriminated very well between weak and significant nocturnal tornadoes, with two-tailed p values on the order of 10^{-5} or better. Estimates from Fig. 8 suggest that 15 m s^{-1} of 5-m AGL storm-relative inflow speed discriminates well between the sampled weak and significant nocturnal tornadoes, and values higher than this threshold indicate an increasing possibility of significant nocturnal tornadoes.

This discriminator can be combined with those found by KS10 to further aid in nocturnal tornado forecasting.

4) CRITICAL ANGLE

The critical angle is the angle between **v** and **c (**EG08**)** and is implicit in the cross product in the $SREH_{0\text{-}1}$. A critical angle of 90-degrees indicates purely streamwise vorticity at the level where **v** is measured. Theoretically, curved low-level hodographs with storm motion toward the center of the hodograph would have critical angles of 90-degrees at each point along the hodograph trace, whereas other shapes such as bent and straight low-level hodographs would have critical angles different than 90-degrees. A critical angle of 90-degrees with **v** defined as the 5-m AGL environmental inflow vector indicates purely streamwise 5-m AGL storm-relative inflow.

Roughly three-quarters of critical angles for nocturnal tornadoes with BH differed from the purely streamwise situation by more than 10-degrees (Fig. 9), and therefore 5-m AGL storm-relative inflow was only fractionally streamwise. As would be expected, critical angles for nocturnal tornadoes with SH were much less streamwise than those associated with BH and CH, with all but three cases more than 40-degrees less than the purely streamwise situation. Surprisingly, nearly half of the critical angles with CH overlapped with those with BH, and only one case was within 10-degrees of the purely streamwise vorticity situation. Thus, CH in this sample did not behave like the ideal curved low-level hodograph and were in general not associated with substantially more streamwise vorticity than were BH. In addition, critical angles discriminated poorly between weak and significant nocturnal torndoes (Fig. 10) and do not appear to be useful as forecasting tools.

c. Nocturnal null events

Markowski et al. (2003; hereafter M03) gathered 40-km RUC-2 proximity soundings for tornadic and nontornadic supercells between 1999 and 2001 (Thompson et al. 2003). While the majority of the cases in M03's sample occurred in the late afternoon or early evening, thirty-four of the nontornadic cases were nocturnal. This subset of nocturnal nontornadic supercells is used herein to construct a sample of nocturnal null events.

Vertical resolution differences between the 40-km and 20-km RUC-2 allow for only cursory comparison between the nocturnal null events from M03's sample and KS10's sample of nocturnal tornadoes. Comparison of soundings from KS10's sample and M03's sample show that, in particular, the 40-km RUC-2 has much coarser vertical resolution in the lowest 100–200 m AGL, and somewhat coarser resolution in the remaining lowest 1500 m AGL, than does the 20-km RUC-2. This is because more vertical levels with fine spacing were added to the 20-km RUC-2 in the lower troposphere (Benjamin et al. 2001). Thus, results from the null cases taken from M03's sample should be regarded as preliminary. However, overall shapes in the lowest 1.5 km AGL from M03 can still be quantified, since the largest differences in vertical resolution between the 40-km and 20-km RUC-2 occur in a very shallow layer next to the surface.

Hodograph shapes for the null cases were evaluated using the same criteria detailed in section 2. Sixteen of the thirty-four nocturnal null cases featured hodographs in the lowest 1.5-km AGL that did not fit any of the three shape categories, and were labeled "unidentifiable." Only nine cases featured BH, with an average bend height of 824 m AGL. Six cases had CH and three had SH. While the nocturnal null cases taken from M03's sample feature coarser resolution near the surface than do the nocturnal tornadoes taken from KS10's sample, and are taken from a different time period, these hodograph shape statistics suggest that there may be a difference in low-level vertical wind shear regimes typically found with tornadic and nontornadic nocturnal severe weather environments. However, these differences must be investigated with a more substantial sample of null events.

d. Comparison with Esterheld and Guiliano (2008)

EG08 noted that many environments with strong speed shear in the 10–500 m AGL layer were associated with bent hodographs, and computed a number of parameters similar to those examined in section 3c herein.

Several differences in EG08's results and the results herein are apparent. Storm-relative inflow speeds at 5-m AGL discriminated well between weak and significant nocturnal tornadoes for the subset of KS10's sample. In contrast, 10-m AGL storm-relative inflow speed discriminated poorly between weak and significant tornadoes for EG08's sample. Additionally, the median 5-m AGL inflow speed from the subset of KS10's sample was stronger by about 5 m s^{-1} than the median 10-m AGL inflow speed for EG08's sample.

EG08 computed their critical angles with the bulk shear vector between 10–500 m AGL, whereas the critical angles for the sample herein were computed with the 5-m AGL environmental wind vector. Despite this difference in critical angle computations, the results between these studies can be compared with confidence. Note that, due to the dominance of unidirectional shear below bend height in the BH examined for the sample herein, the 5-m AGL environmental wind vector is nearly parallel to the bulk shear vector below bend height. For completeness, the authors also computed the bulk shear vector between 5-m AGL and the bend height to produce measurements similar to the 10–500 m AGL bulk shear vector computed in EG08. The resulting bulk shear vectors were identical or nearly identical to the 5-m AGL environmental wind vector in every case.

The most striking differences between the results herein and EG08's results were for the critical angles. EG08 found that critical angles for both weak and significant tornadoes with bent low-level hodographs were centered on 90-degrees (Fig. 13 of EG08) and therefore that the 10-m AGL inflow was nearly streamwise in most cases. In the subset of KS10's sample, however, the majority of both weak and significant tornadoes with BH were removed from the purely streamwise situation by at least 10-degrees (Fig. 9) and therefore in some cases a sizable portion of the 5-m AGL inflow was not streamwise.

Differences between the critical angle results presented in Sec. 3c and those in EG08 may be rooted in differences in sampling criteria. EG08's sample was of similar size to the sample analyzed herein, but was mainly comprised of afternoon tornadoes. Their results were based on observed storm motion and inflow measured by the Oklahoma Mesonet, whereas the sample herein was based on RUC-2 model data with storm motion computed via the Internal Dynamics Technique. It is likely that using the Internal Dynamics Technique to compute storm motion contributed to some error to both the 5-m AGL storm-relative inflow speed and critical angle computations performed on the subset of KS10's sample.

4. Connection between the low-level jet and low-level hodograph bends

Given that LLJs correlated well with the large bulk vertical wind shear in the lowest kilometer and below bend height, one might expect that the hodograph bends that mark the terminus of layers of speed shear adjacent to the surface would be located near the heights of jet maxima. However, the heights of jet maxima correlated poorly with the heights of low-level hodograph bends (.24). Thus, it appears that the formation of bent hodographs is dependent on factors other than LLJs that might provide additional strong shallow speed shear. Since the majority of LLJs in this study were embedded in strong dynamic systems (KS10) rather than purely driven by the inertial oscillation, it seems possible that associated mesoscale structures such as frontal boundaries could have also contributed to strong shallow speed shear.

5. Summary and conclusions

Vertical shear of the horizontal wind is necessary for tornadic supercells to form and persist. Typically, vertical wind shear in severe weather environments is characterized as extending in a spectrum between the extremes of pure speed shear and pure directional shear (Weisman and Klemp 1982, 1984). Hodograph shape is a function of the vertical wind shear and can bear much light on the type and magnitude of vertical wind shear in which supercells and tornadoes occur.

Nocturnal tornadoes are associated with much stronger vertical wind shear than are daytime tornadoes (KS10). Hodograph shape was examined herein for a subset of KS10's sample in effort to gain further insight into the sheared environments in which nocturnal tornadoes often form. Preliminary review revealed that many of the sampled nocturnal tornadoes occurred in proximity of hodographs similar to the bent low-level hodographs of TE00, M06, and EG08 that often separated a layer of strong speed shear next to the surface from strong directional shear above in the free atmosphere. For a subset of KS10's sample of nocturnal tornadoes with RUC-2 proximity soundings, vertical wind shear in the lowest 1.5-km AGL was quantified in an attempt to categorize low-level hodograph shapes into the archetypes of bent, curved, and straight hodographs. Shape categories were based on theories of ideal hodograph shapes and the sheared environments in which they occur.

Analysis of low-level hodograph shapes allows for investigation of the shear regimes in which different shapes typically occur. The regime that often produces bent low-level hodographs is often characterized by dominant speed shear in a shallow layer above the surface, and dominant directional shear in the above layer. The definition employed in this study to identify bent low-level hodographs allows for some directional shear below hodograph bends, and some speed shear above hodograph bends, yet effectively captures the regime of interest. The effect is not merely to identify a hodograph shape common to nocturnal tornado environments, but to identify the vertical wind shear regime that often characterizes nocturnal tornado proximity environments and examine its effects on low-level rotation.

Nearly three-quarters of the sampled nocturnal tornadoes occurred in proximity of bent hodographs in the lowest 1.5-km AGL, while less than 5% of the sampled nocturnal tornadoes were associated with curved low-level hodographs similar to the generally accepted climatological hodograph for tornadoes (Maddox 1976). Nearly 90% of the strong speed shear layers were less than 1-km deep, and shear strengths correlated very well with the maximum speeds of overhead LLJs.

SREH is directly related to vertical wind shear, and $SREH_{0\text{-}1}$ varied among the hodograph shapes categorized herein. BH and SH were associated with much larger $SREH_{0\text{-}1}$ than CH. While SH had much larger 5-m AGL storm-relative inflow and 0–1 km AGL bulk shear that contributed to $SREH_{0\text{-}1}$, BH were much more streamwise than were SH in the nocturnal boundary layer and above. Thus, it appears that different factors that affect $SREH_{0\text{-}1}$ are at play for different low-level hodograph shapes. In addition, cursory examination of a sample of nocturnal null events suggests that bent low-level hodographs may indicate heightened nocturnal tornadic potential. However, the sample of nocturnal null events examined was too compromised to draw clear connections.

Acceptance of the curved low-level hodograph as the climatological norm for tornadic environments is based on studies that are biased toward daytime/early-evening tornadoes (e.g.

Maddox 1976, Markowski et al. 2003). Despite its prevalence in nocturnal tornadic environments, the bent low-level hodograph has been largely ignored in the literature, with the exceptions of TE00, M06, and EG08. The authors suggest that the bent low-level hodograph be used as the climatological norm for nocturnal tornadoes and the curved low-level hodograph be retained as the climatological norm for daytime tornadoes. The use of these separate hodographs will emphasize that daytime tornadoes tend to occur in environments with strong veering of the winds next to the surface while nocturnal tornadoes tend to occur in environments with sharp changes in wind speeds over shallow depths.

While the bent hodograph shape is often connected to strong speed shear in shallow layers adjacent to the surface, its exact cause remains unknown. Future studies will include high-resolution simulations of bent, curved, and straight low-level hodographs to examine the influence of hodograph shape on tornado dynamics. Numerical simulations of storms in environments with bent low-level hodographs in particular will be focused on in the same vein as Weisman and Klemp (1982, 1984).

Acknowledgements The authors would like to thank Jason Levit of the Storm Prediction Center for his help in retrieving archived RUC-2 data. This work was supported by the National Science Foundation (NSF) grant ATM-0733539.

APPENDIX A

The shear-based criteria described in Sec. 2 for identifying a bend in the lowest 1.5-km AGL of hodographs have to be met in adaptive layer rather than in a fixed layer in order to correctly identify the vertical height at which directional shear becomes dominant.

At each measurement level, the wind direction was converted from degrees to radians, and the average wind direction in radians in the lowest 1.5-km AGL was computed. For each measurement level below 1.5-km AGL, the difference in wind direction at that height and the 1.5-km AGL-average wind direction was computed. This difference, when multiplied by the change in wind speed between the measurement level and adjacent lower measurement level and divided by the change in height between the measurement level and adjacent lower measurement level, gave the directional shear averaged over the 1.5-km AGL layer in units of s^{-1}.

At each measurement level, speed shear was computed as the change in wind speed between the measurement level and adjacent lower measurement level divided by the change in height between the measurement level and adjacent lower measurement level. The dimensionless ratio of speed shear to directional shear was then computed at each level and averaged below 1.5-km AGL.

Wind direction was averaged for sequentially smaller depths at measurement levels below 1.5-km AGL, and the above process was repeated at each measurement level. Ratios of averaged speed shear to averaged directional shear were re-computed over corresponding sequentially smaller depths. Those hodographs with averaged ratios of speed to directional shear greater than or equal to 10 continuously at each measurement level below 1.5-km AGL indicated that speed shear was on average at least an order of magnitude greater than directional shear at each measurement level below 1.5-km AGL, and were categorized as straight hodographs.

Those hodographs with averaged ratios of speed to directional shear less than 10 continuously at each measurement level below 1.5-km AGL indicated that directional shear was on average at least an order of magnitude greater than speed shear at each measurement level below 1.5-km AGL, and were categorized as curved hodographs. Those hodographs in which the averaged ratios of speed to directional shear were greater than or equal to 10 continuously at each measurement level in a layer adjacent to the surface, topped above by a layer in which the averaged ratios of speed to directional shear were greater less than 10 continuously through a layer, indicated that a layer of dominant speed shear was topped by a layer of dominant directional shear. Such hodographs were categorized as bent hodographs.

REFERENCES

Ashley, W. S., A. J. Krmenec, and R. Schwantes, 2008: Vulnerability due to nocturnal tornadoes. *Wea. Forecasting*, **23**, 795–807.

Benjamin, S. G., G. A. Grell, S. S. Weygandt, T. L. Smith, T. G. Smirnova, B. E. Schwartz, D. Kim, D. Devenyi, K.J. Brundage, J.M. Brown, and G.S. Manikin, 2001: The 20-km version of the RUC. Preprints, *14th Conf. Num. Wea. Pred.*, Ft. Lauderdale, FL, Amer. Meteor. Soc., J75–79.

Bunkers M. J., B. A. Klimowski, J. W. Zeitler, R. L. Thompson, and M. L. Weisman, 2000: Predicting supercell motion using a new hodograph technique. *Wea. Forecasting*, **15**, 61–79.

Craven, J. P., and H. E. Brooks, 2004: Baseline climatology of sounding derived parameters associated with deep moist convection. *Natl. Wea. Dig.*, **28** (December), 13–24.

Davies, J. M., and R. H. Johns, 1993. Some wind and instability parameters associated with strong and violent tornadoes. Part 1. Wind shear and helicity. *The Tornado: Its Structure, Dynamics, Prediction, and Hazards, Geophys. Monogr.*, No. 79, Amer. Geophys. Union, 573-582.

Davies-Jones, R., 1984: Streamwise vorticity: The origin of updraft rotation in supercell thunderstorms. *J. Atmos. Sci.*, **41**, 2991–3006.

——, D. Burgess, and M. Foster, 1990: Test of helicity as a tornado forecast parameter. Preprints, *16th Conf. on Severe Local Storms*, Kananaskis, AB, Canada, Amer. Meteor. Soc., 588 – 592.

French, A. J., and M. D. Parker, 2010: The response of simulated nocturnal convective systems to a developing low-level jet. *J. Atmos. Sci*. doi: 10.1175/2010JAS3329.1

Esterheld, J. M., and D. J. Guiliano, 2008: Discriminating between tornadic and nontornadic supercells: A new hodograph Technique. *Electronic J. Severe Storms Meteor*., **3**, 1–50.

Grasso, L. D., and W. R. Cotton, 1993: Numerical simulation of a tornado vortex. *J. Atmos. Sci,* **52**, 1192–1203.

Hart, J. A., and J. Korotky, 1991: The NSHARP workstation v1.50, A skew-t/hodograph analysis and research program for the IBM and compatible PC, user's manual. National Weather Service, National Oceanic and Atmospheric Administration, U.S. Department of Commerce, 62 pp.

Johns, R. H., J. M. Davies, and P. W. Leftwich, 1993: Some wind and instability parameters associated with strong and violent tornadoes. Part II: Variations in the combinations of wind and instability parameters. *The Tornado: Its Structure, Dynamics, Prediction, and Hazards, Geophys. Monogr.,* **79,** 583-590.

Kis, A. K., and J. M. Straka: Nocturnal tornado climatology. *Wea. Forecasting*, **25**, 545–561.

Klemp, J. B., 1987: Dynamics of tornadic thunderstorms. *Annu. Rev. Fluid Mech.*, **19**, 369–402.

——, and R. B. Wilhelmson, 1978: The simulation of three-dimensional convective storm dynamics. *J. Atmos. Sci.*, **35**, 1070 – 1096.

Maddox, R. A., 1976: An evaluation of tornado proximity wind and stability data. *Mon. Wea. Rev.*, **104**:133–142.

——, 1993: Diurnal low-level wind oscillation and storm-relative helicity. *The Tornado: Its Structure, Dynamics, Prediction, and Hazards, Geophys. Monogr.*, No. 79, Amer. Geophys. Union, 591–598.

Markowski, P., and Y. Richardson, 2006: On the classification of vertical wind shear as directional shear versus speed shear. *Wea. Forecasting*, **21**, 242–247.

——, C. Hannon, J. Frame, E. Lancaster, A. Pietrycha, R. Edwards, and R. Thompson, 2003: Characteristics of vertical wind profiles near supercells obtained from the Rapid Update Cycle. *Wea. Forecasting*, **18**, 1262–1272.

Miller, D. J., 2006: Observations of low level thermodynamic and wind shear profiles on significant tornado days. Preprints, *23rd Conf. on Severe Local Storms*, St. Louis, MO, Amer. Meteor. Soc., 1206 – 1223.

Ramsay, H. A., and C. A. Doswell, 2005: A sensitivity study of hodograph-based methods for estimating supercell motion. *Wea. Forecasting*, **20**, 954–970.

Rasmussen, E. N., 2003: Refined supercell and tornado forecast parameters. *Wea. Forecasting*, **18**, 530–535.

——, and D. O. Blanchard, 1998: A baseline climatology of sounding-derived supercell and tornado forecast parameters. *Wea. Forecasting*, **13**, 1148–1164.

Rotunno, R., and J. B. Klemp, 1982: The influence of the shear-induced pressure gradient on thunderstorm motion. *Mon. Wea. Rev.*, **110**, 136–151.

——, and ——, 1985: On the rotation and propagation of simulated supercell thunderstorms. *J. Atmos. Sci.*, **42**, 271–292.

Stull, R. B., 1988: *An Introduction to Boundary Layer Meteorology*. Kluwer Academic, 666 pp.

Thompson, R. L., and R. Edwards, 2000: An overview of the environmental conditions and forecast implications of the 3 May 1999 tornado outbreak. *Wea. Forecasting*, **15**, 682 – 699.

——, ——, J. A. Hart, K. L. Elmore, and P. Markowski, 2003: Close proximity soundings within supercell environments obtained from the Rapid Update Cycle. *Wea. Forecasting*, **18**, 1243–1261.

——, C. M. Mead, and R. Edwards, 2007: Effective storm-relative helicity and bulk shear in supercell thunderstorm environments. *Wea. Forecasting*, **22**, 102–115.

Weisman, M. L., and J. B. Klemp, 1982: The dependence of numerically simulated convective storms on vertical wind shear and buoyancy. *Mon. Wea. Rev*., **110**, 504 – 520.

——, and J. B. Klemp, 1984: The structure and classification of numerically simulated convective storms in directionally varying wind shears. *Mon. Wea. Rev*, **112**:2479–2498.

——, and ——, 1986: Characteristics of isolated convective storms. Mesoscale Meteorology and Forecasting, P. S. Ray, Ed., Amer. Meteor. Soc., 331–358.

——, and R. Rotunno, 2000: The use of vertical wind shear versus helicity in interpreting supercell dynamics. *J. Atmos. Sci*., **57**, 1452–1472.

Whiteman, C. D., X. Bian, and S. Zhong, 1997: Low-level jet climatology from enhanced rawinsonde observations at a site in the Southern Great Plains. *J. Appl. Meteor*., **36**, 1363–1376.

Wicker, L. J., 1996: The role of near surface wind shear on low-level mesocyclone generation and tornadoes. Preprints, *18th Conf. on Severe Local Storms*, San Fransisco, CA, Amer. Meteor. Soc., 115–119.

——, and R. B. Wilhelmson, 1993: Numerical simulation of tornadogenesis within a supercell thunderstorm. The tornado: Its structure, dynamics, prediction, and hazards. AGU Monograph Series, C. R. Church (Ed.). 79, 75-88.

——, and ——, 1995: Simulation and analysis of tornado development and decay within a three-dimensional supercell thunderstorm. *J. Atmos. Sci*, **52**, 2675–2703.

P6.9

Date	Time	State	Strength	Station I.D.	Hodograph shape
03/06/04	0955 (0327)	AL	F0	KHSV	TRANSITION
03/06/04	1000 (0332)	AL	F0	KHSV	TRANSITION
04/12/04	0635 (1104)	FL	F0	KFMY, KRSW	bent
04/23/04	1013 (0325)	AR	F0	RUE	bent
05/01/04	1243 (0600)	AR	F0	FLP	bent
05/01/04	0427 (0924)	MO	F1	KCGI, P#R	TRANSITION
05/26/04	0655 (0734)	VA	F0	KTRI	TRANSITION
08/02/04	0337 (0904)	MN	F1	KAXN, C24	bent
08/06/04	0523 (1101)	SD	F0	P#7	bent
08/06/04	0606 (1139)	SD	F0	P#7	bent
08/06/04	0610 (1145)	SD	F1	P#7	bent
08/06/04	0612 (1145)	SD	F0	P#7	bent
08/06/04	0614 (1149)	SD	F0	P#7	bent
08/06/04	0615 (1149)	SD	F0	P#7	bent
08/27/04	0936 (0308)	MO	F0	KSTJ, P#I	bent
08/27/04	1049 (0419)	MO	F0	P#I	bent
11/11/04	1237 (0704)	AR	F0	RUE	bent
12/09/04	0404 (1006)	MS	F1	CLN, KPIB	bent
12/29/04	1221 (0815)	CA	F0	KSNA	bent
03/08/05	0927 (0315)	FL	F0	AQQ	bent
04/23/05	0318 (0755)	FL	F0	CTY	UNIDENTIFIABLE
04/30/05	0335 (0830)	MS	F0	CLN, KPIB	TRANSITION
04/30/05	0429 (0916)	AL	F0	KCKL, BMX	bent
04/30/05	0520 (1004)	AL	F1	BMX	bent
05/20/05	1257 (0525)	VA	F1	FRI	bent
06/01/05	1119 (0455)	TX	F0	G#4	bent
06/01/05	0232 (0804)	TX	F0	KSAT, SAT	bent
06/05/06	0933 (0301)	IA	F0	KSUX	bent
06/08/05	1033 (0407)	SD	F0	KATY, WTT	bent
06/08/05	1034 (0410)	ND	F0	KABR	bent
06/08/05	1044 (0419)	SD	F1	KABR	TRANSITION
06/19/05	0355 (0945)	ND	F1	KP11, C22	bent
06/19/05	0405 (0955)	ND	F1	KP11, C22	bent
06/19/05	0426 (1015)	ND	F1	C22	bent
07/06/05	0643 (1119)	AL	F0	KGZH	bent
07/06/05	0645 (1219)	AL	F0	KPNS	bent
07/11/05	0916 (0255)	ND	F0	C22, KJMS, KP11	bent
07/11/05	0923 (0300)	ND	F0	C22, KJMS, KP11	bent
07/11/05	1033 (0410)	ND	F1	KP11	bent
07/26/05	1247 (0534)	MI	F1	KRQB, KGRR	TRANSITION
08/31/05	1211 (0422)	PA	F1	W54	bent
08/31/05	1227 (0437)	PA	F1	W54	bent
08/31/05	1229 (0440)	PA	F1	W54	bent

10/22/05	0305 (0700)	NC	F0	KMHX	UNIDENTIFIABLE
12/04/05	1045 (0502)	AR	F0	KGLH	bent
12/25/05	1118 (0445)	FL	F0	KPFN	bent
12/26/05	0233 (1045)	CA	F0	KMCE, CCL, GLRY	TRANSITION
03/11/06	1150 (0612)	OK	F1	C04, P#V	bent
04/22/06	1024 (0336)	MS	F0	CLN, KPIB	curved
05/08/06	0946 (0316)	MN	F0	KBJI	bent
05/09/06	1027 (0316)	LA	F1	6RO, KNEW	TRANSITION
10/04/06	1145 (0410)	MI	F1	KCAD	bent
10/16/06	0332 (0845)	TX	F1	KVCT	curved
10/16/06	0502 (1007)	TX	F0	KGLS	bent
10/16/06	0648 (1200)	TX	F0	KPBT	bent
12/30/06	0632 (1243)	LA	F1	KLFT	bent

Table 1: Sampled weak nocturnal tornadoes. Time is given in Local Solar Time with UTC equivalent in parentheses. RUC-2 surface observing site identifiers are according to the NSHARP format (Hart and Korotoky 1991). Hodograph shapes are as defined in the text. Additional information is found in Tables S4 and S5 of Kis and Straka (2010).

Date	Time	State	Strength	Station I.D.	Hodograph shape
05/30/04	1004 (0330)	MO	F4	P#I	bent
11/24/04	0927 (0400)	TX	F2	KLFK	curved
11/24/04	1240 (0654)	MS	F2	CLN, KPIB	bent
11/24/04	0102 (0715)	MS	F2	CLN	bent
11/24/04	0140 (0752)	MS	F2	CLN, KPIB	bent
11/24/04	0547 (1148)	AL	F2	KMGM	bent
11/24/04	624 (1224)	AL	F2	KMGM	bent
01/08/05	0949 (0334)	MS	F2	KGPT	bent
11/06/05	1001 (0419)	MO	F2	KJBR	bent
11/06/05	1021 (0438)	AR	F2	KJBR	bent
11/06/05	1022 (0440)	AR	F2	KJBR	bent
11/06/05	0141 (0746)	KY	F3	KBWG	bent
01/13/06	1009 (0428)	AR	F2	KHOT	bent
03/13/06	0904 (0308)	OK	F3	KFYV	straight
03/13/06	0934 (0337)	OK	F3	KFYV	TRANSITION
03/13/06	1009 (0410)	AR	F2	KFYV	bent
03/13/06	1016 (0415)	MO	F3	UMN	bent
03/13/06	1018 (0416)	MO	F3	KSGF, P#H	TRANSITION
03/13/06	1024 (0419)	MO	F2	P#H	TRANSITION
03/13/06	1211 (0600)	MO	F3	KSUS	bent
03/13/06	1238 (0630)	MO	F2	KSUS	bent
03/13/06	0130 (0719)	MO	F3	KSUS	bent
04/08/06	0303 (0730)	GA	F2	KFTY	straight
05/06/08	1210 (0545)	TX	F2	KACT	bent
10/17/06	0333 (0839)	MS	F2	KPIB	straight
11/15/06	0241 (0849)	LA	F2	KMCB	bent
11/16/06	1107 (0422)	NC	F2	KCLT	straight
11/16/06	0633 (1137)	NC	F3	ILM, KILM	straight

Table 2: As in Table 1, but for sampled significant nocturnal tornadoes. Additional information is found in Tables S1, S2, and S3 of Kis and Straka (2010).

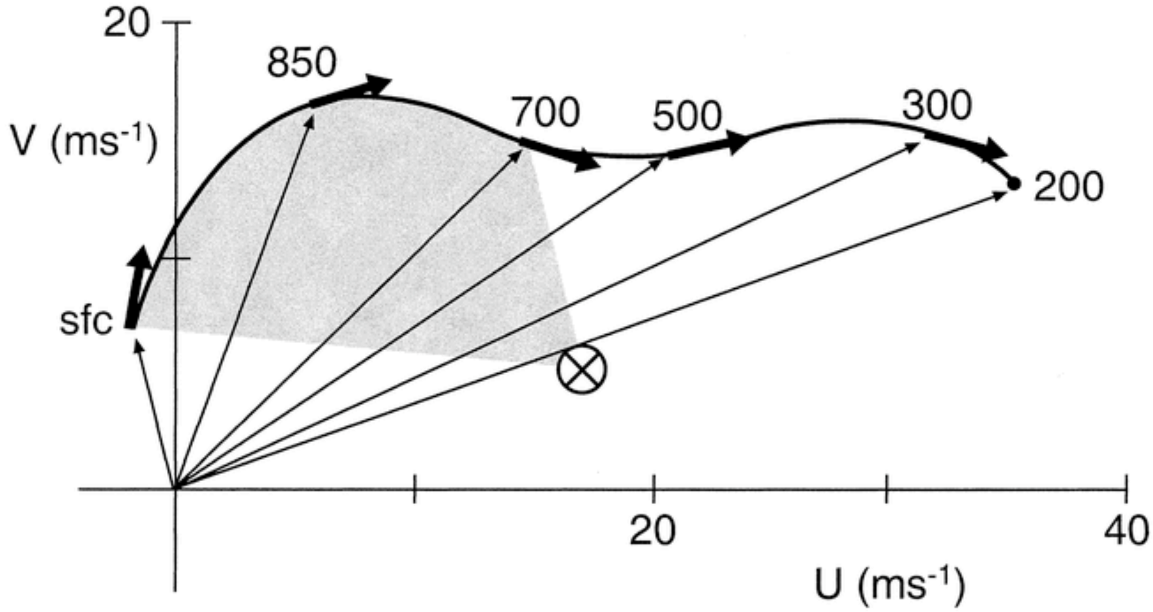

FIG. 1: Mean sounding for tornado outbreaks (adapted from Maddox 1976 by Weisman and Rotunno 2000).

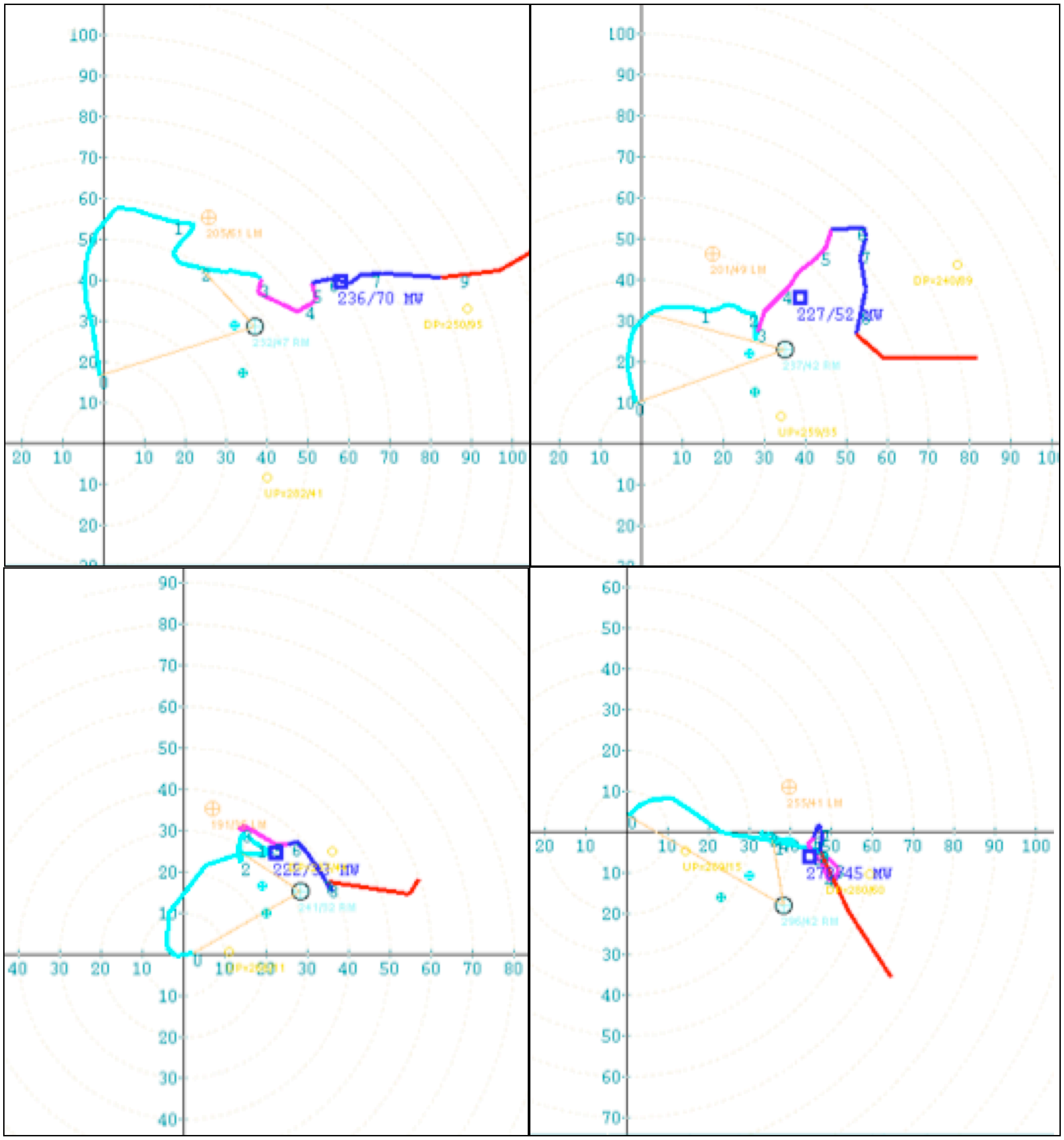

FIG. 2: Examples of bent hodographs in the lowest 1.5-km AGL with (top left) straight speed shear layers and (top right) slightly curved speed shear layers below hodograph bends. Examples of (bottom left) curved and (bottom right) straight hodographs in the lowest 1.5-km AGL.

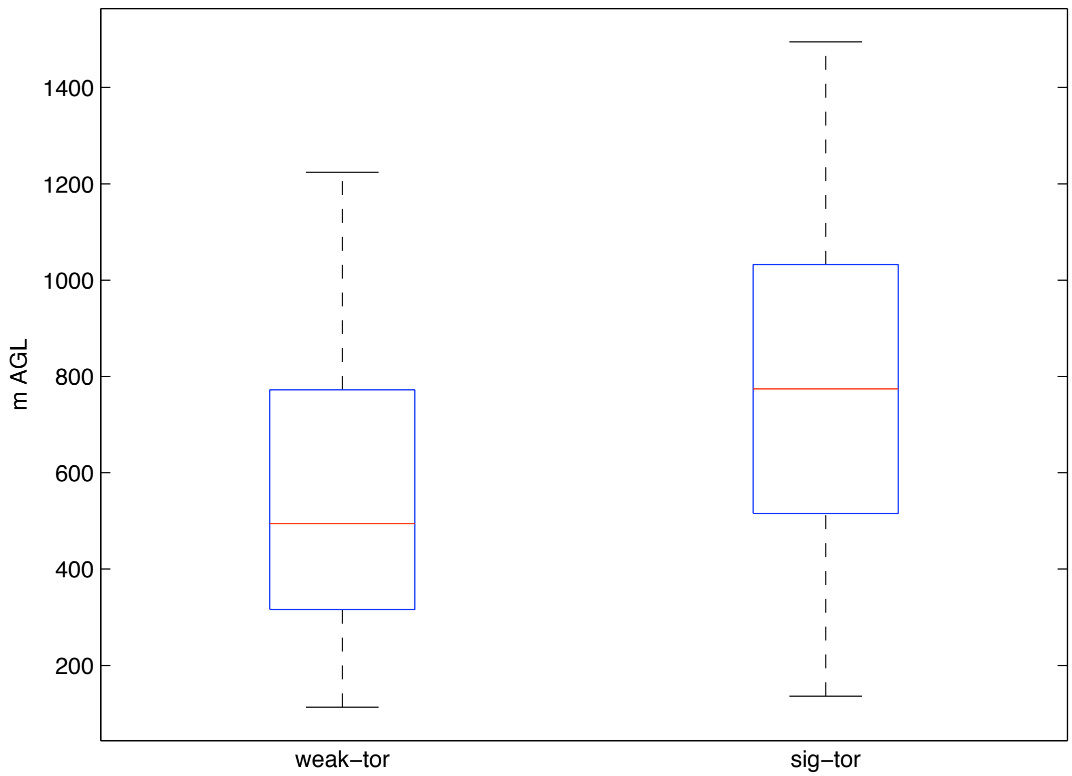

FIG. 3: Box plots of hodograph bend height (m AGL) for sampled (left) weak and (right) significant nocturnal tornadoes with bent hodographs (BH) in the lowest 1.5 km AGL. The blue box extends from the first quartile (25th percentile) to the third quartile (75th percentile) (interquartile range), and the red line is the median value. The lower error bar extends to the smallest data value that is greater than or equal to 1.5 x (interquartile range) below the first quartile, and the upper error bar extends to the largest data value that is less than or equal to 1.5 x (interquartile range) above the third quartile. Red plus signs are outliers.

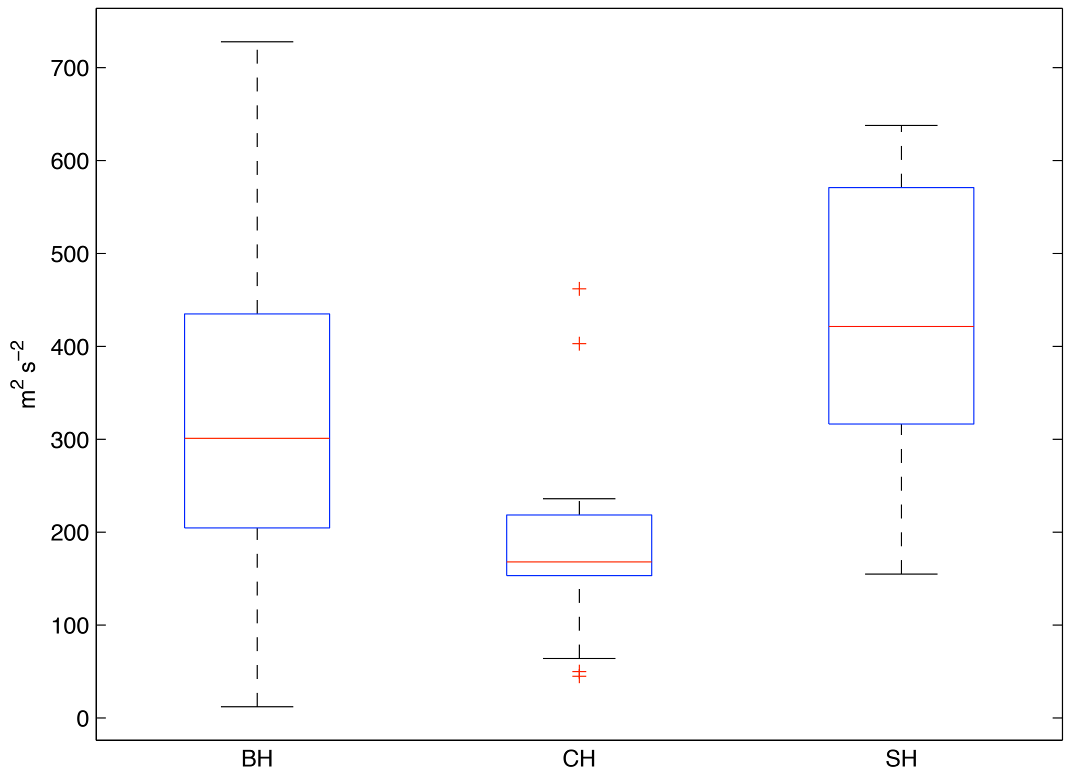

FIG. 4: Box plots of storm relative environmental helicity (m^2 s^{-2}) in the lowest kilometer ($SREH_{0-1}$). Box plots are formatted as in Fig. 3.

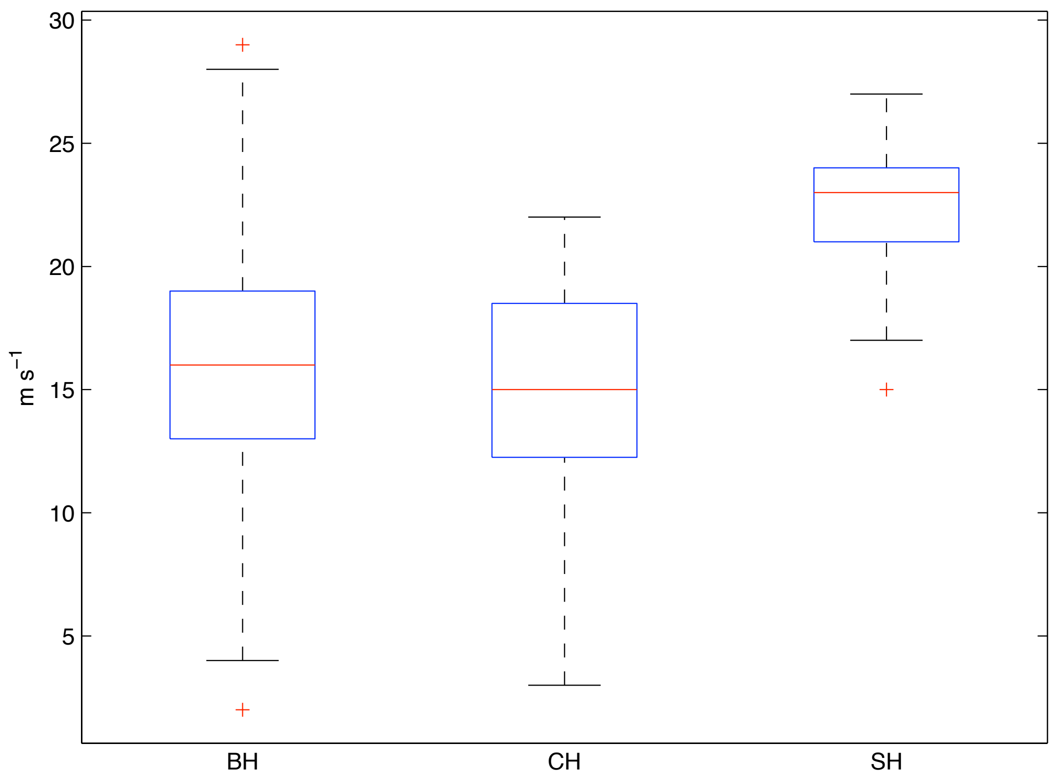

FIG. 5: Box plots of 0–1 km AGL bulk vertical wind shear (m s^{-1}) for sampled nocturnal tornadoes with bent (BH), curved (CH), and straight (SH) hodographs below 1.5-km AGL. Box plots are formatted as in Fig. 3.

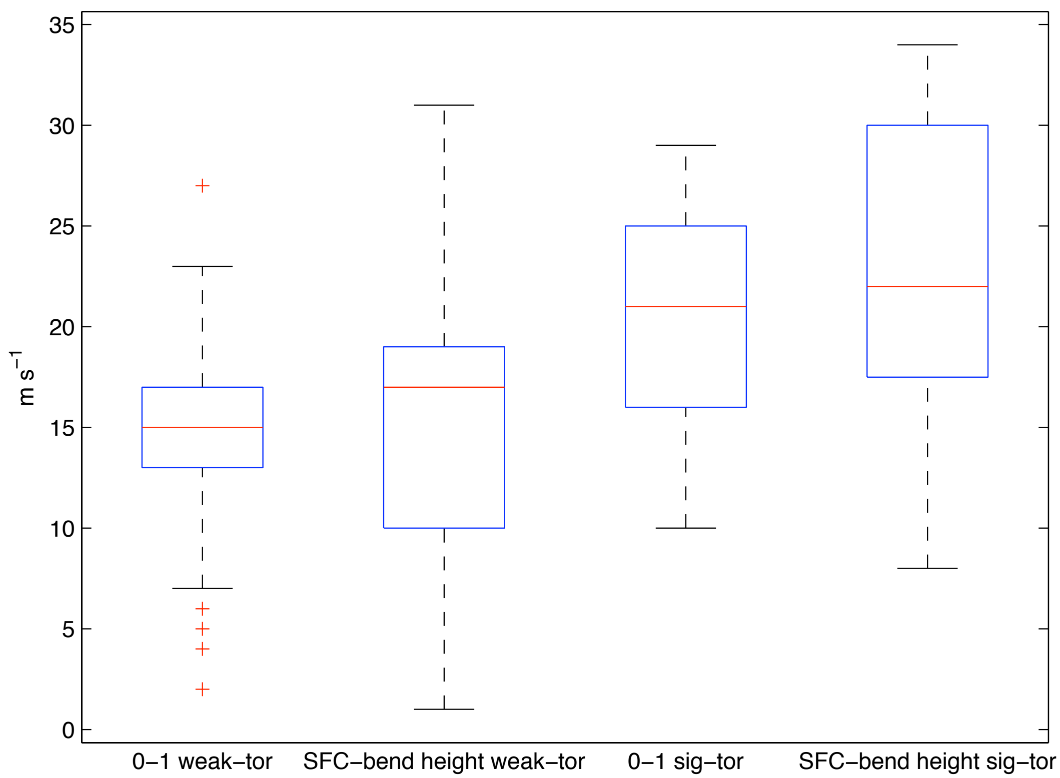

FIG. 6: Box plots of 0–1 km AGL and SFC–bend bulk vertical wind shear (m s^{-1}) for sampled nocturnal tornadoes with BH in the lowest 1-km AGL. Box plots are formatted as in Fig. 3.

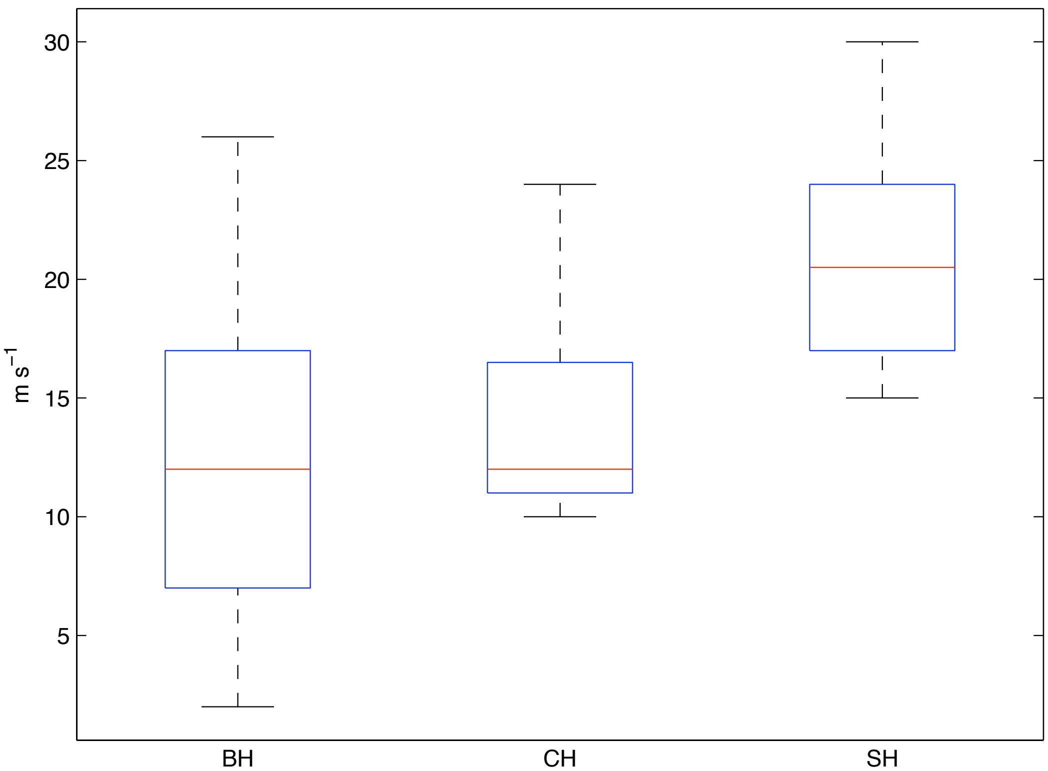

FIG. 7: Box plots of 5-m AGL storm-relative inflow speed (m s^{-1}) for sampled nocturnal tornadoes with bent (BH), curved (CH), and straight (SH) hodographs below 1.5-km AGL. Box plots are formatted as in Fig. 3.

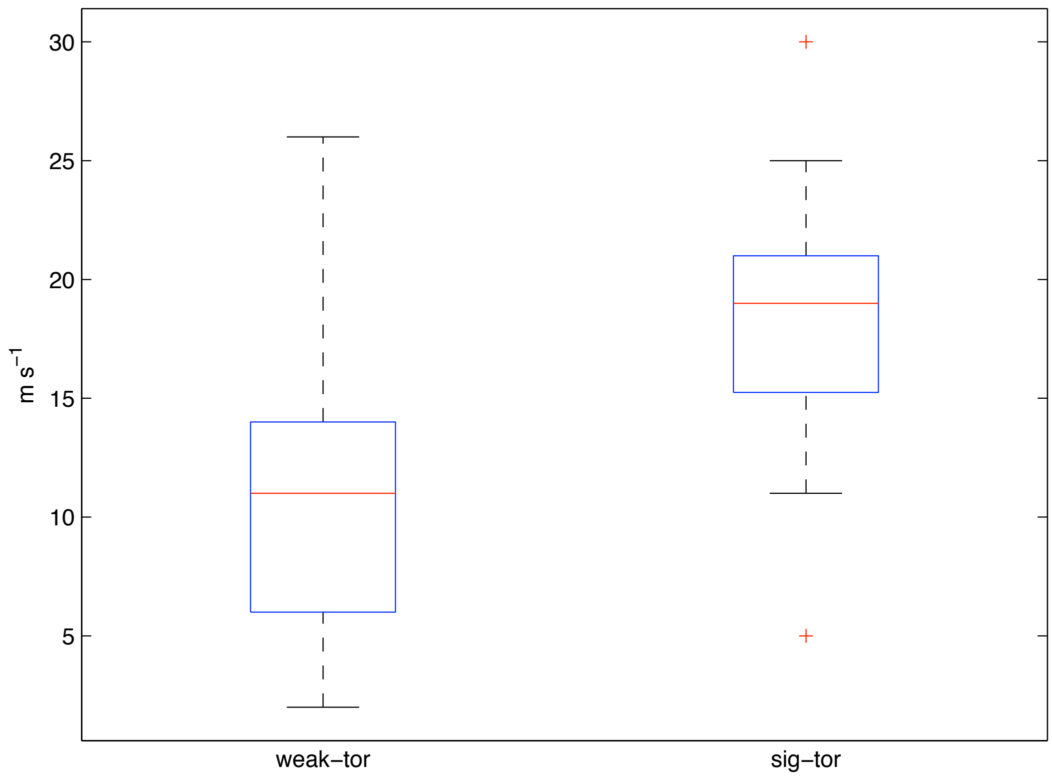

FIG. 8: Box plots of 5-m AGL storm-relative inflow speed (m s^{-1}) for sampled (left) weak and (right) significant nocturnal tornadoes. Box plots are formatted as in Fig. 3.

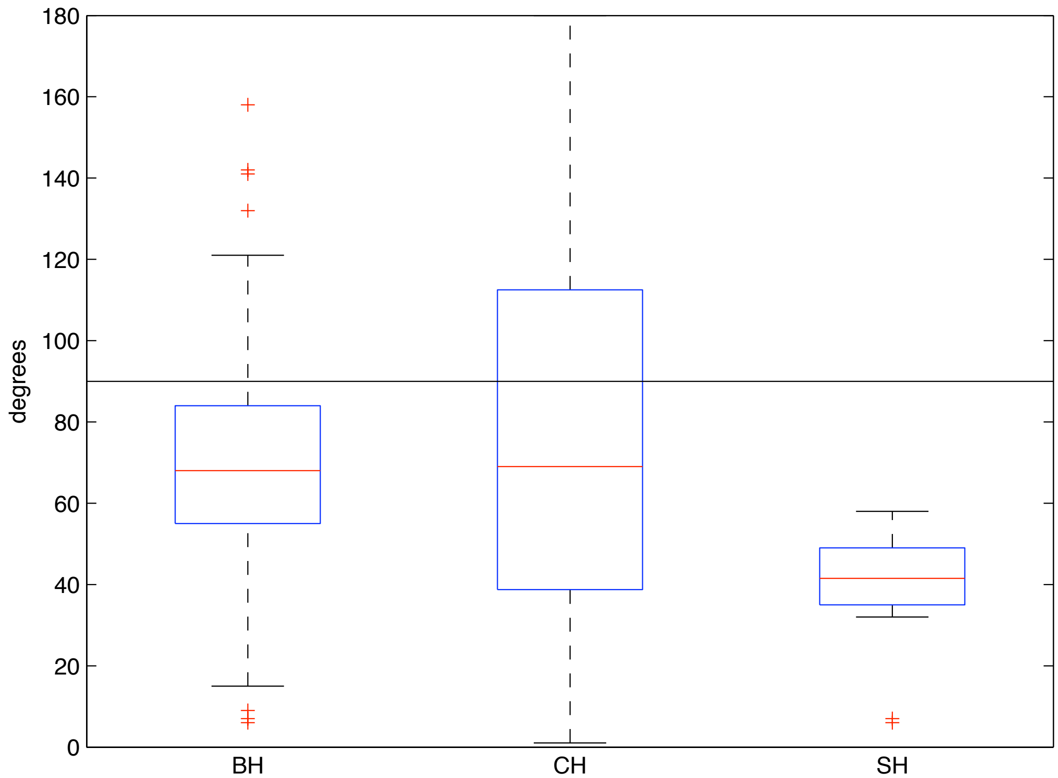

FIG. 9: Box plots of critical angles (degrees) computed with the 5-m AGL environmental inflow vector for sampled nocturnal tornadoes with bent (BH), curved (CH), and straight (SH) hodographs below 1.5-km AGL. Box plots are formatted as in Fig. 3. The solid black line indicates the purely streamwise situation of 90 degrees.

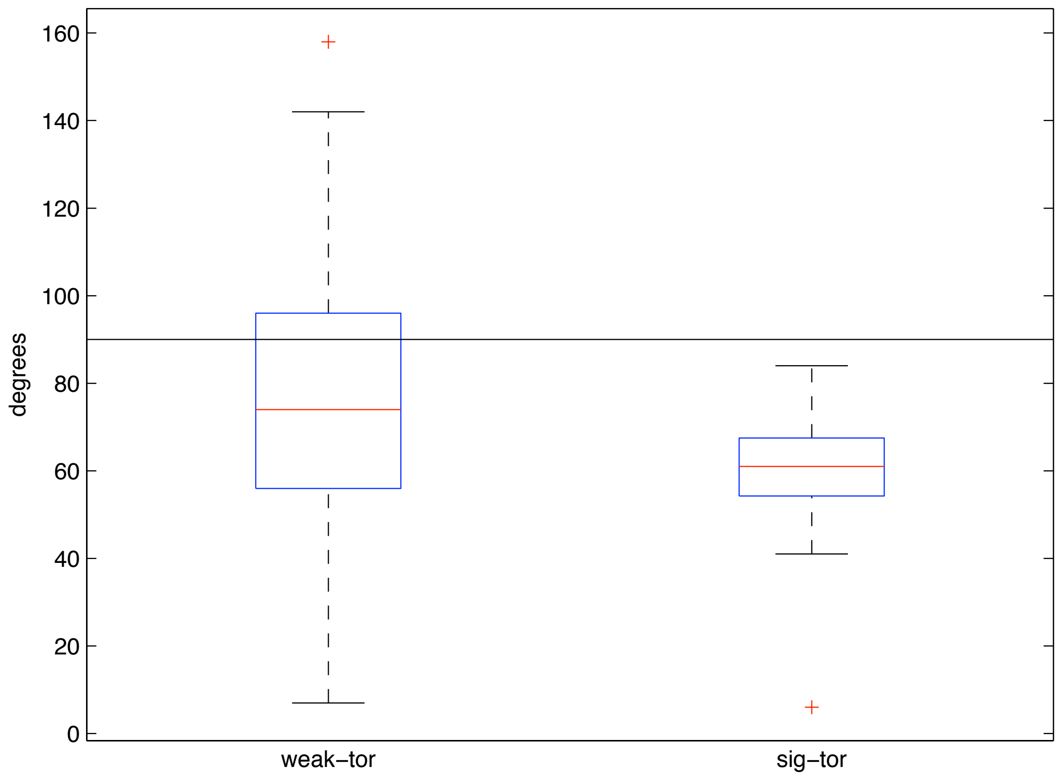

FIG. 10: Box plots of critical angles (degrees) computed with the 5-m AGL environmental inflow vector for sampled weak and significant nocturnal tornadoes. Box plots are formatted as in Fig. 3. The solid black line indicates the purely streamwise situation of 90 degrees.